

# Deconstructing pathological tau by biological process in early stages of Alzheimer disease: a method for quantifying tau spatial spread in neuroimaging



Stephanie Doering, Austin McCullough, Brian A. Gordon, Charles D. Chen, Nicole McKay, Diana Hobbs, Sarah Keefe, Shaney Flores, Jalen Scott, Hunter Smith, Stephen Jarman, Kelley Jackson, Russ C. Hornbeck, Beau M. Ances, Chengjie Xiong, Andrew J. Aschenbrenner, Jason Hassenstab, Carlos Cruchaga, Alisha Daniels, Randall J. Bateman, the Dominantly Inherited Alzheimer Network (DIAN) Investigators, John C. Morris, and Tammie L. S. Benzinger\*



Washington University in Saint Louis School of Medicine, Saint Louis, MO, USA

## Summary

**Background** Neuroimaging studies often quantify tau burden in standardized brain regions to assess Alzheimer disease (AD) progression. However, this method ignores another key biological process in which tau spreads to additional brain regions. We have developed a metric for calculating the extent tau pathology has spread throughout the brain and evaluate the relationship between this metric and tau burden across early stages of AD.

**Methods** 445 cross-sectional participants (aged  $\geq 50$ ) who had MRI, amyloid PET, tau PET, and clinical testing were separated into disease-stage groups based on amyloid positivity and cognitive status (older cognitively normal control, preclinical AD, and symptomatic AD). Tau burden and tau spatial spread were calculated for all participants.

**Findings** We found both tau metrics significantly elevated across increasing disease stages ( $p < 0.0001$ ) and as a function of increasing amyloid burden for participants with preclinical ( $p < 0.0001$ ,  $p = 0.0056$ ) and symptomatic ( $p = 0.010$ ,  $p = 0.0021$ ) AD. An interaction was found between tau burden and tau spatial spread when predicting amyloid burden ( $p = 0.00013$ ). Analyses of slope between tau metrics demonstrated more spread than burden in preclinical AD ( $\beta = 0.59$ ), but then tau burden elevated relative to spread ( $\beta = 0.42$ ) once participants had symptomatic AD, when the tau metrics became highly correlated ( $R = 0.83$ ).

**Interpretation** Tau burden and tau spatial spread are both strong biomarkers for early AD but provide unique information, particularly at the preclinical stage. Tau spatial spread may demonstrate earlier changes than tau burden which could have broad impact in clinical trial design.

**Funding** This research was supported by the Knight Alzheimer Disease Research Center (Knight ADRC, NIH grants P30AG066444, P01AG026276, P01AG003991), Dominantly Inherited Alzheimer Network (DIAN, NIH grants U01AG042791, U19AG03243808, R01AG052550-01A1, R01AG05255003), and the Barnes-Jewish Hospital Foundation Willman Scholar Fund.

**Copyright** © 2024 Published by Elsevier B.V. This is an open access article under the CC BY-NC-ND license (<http://creativecommons.org/licenses/by-nc-nd/4.0/>).

**Keywords:** Alzheimer disease; Positron emission tomography; Tau spread; Tau propagation

## Introduction

Alzheimer disease (AD) is a neurodegenerative disease characterized by the accumulation of amyloid-beta plaques and tau neurofibrillary tangles (NFTs) as well as subsequent neurodegeneration and cognitive decline.<sup>1-4</sup> Amyloid-beta has long been thought to be a driving initial factor of AD<sup>5</sup> as plaques begin developing,<sup>3,6</sup> and spread extensively,<sup>7-9</sup> decades before the presentation of

clinical symptoms.<sup>10</sup> The presence of NFTs occurs later in the disease course and is shown to be tightly coupled with neurodegeneration and cognitive impairment.<sup>11-18</sup> Given its prominent role in the transition to an impaired state understanding tauopathy is of utmost importance.

Early histopathological studies found a progressive spatial pattern for NFTs beginning in the entorhinal

\*Corresponding author. Washington University School of Medicine in St. Louis, Mallinckrodt Institute of Radiology, Box 8131, Neuroimaging Laboratories Research Center (NIL-RC), 4525 Scott Ave., Room 2115, St. Louis, MO 63110, USA.

E-mail address: [benzingert@wustl.edu](mailto:benzingert@wustl.edu) (T.L.S. Benzinger).

### Research in context

#### Evidence before this study

We searched PubMed up to April 13, 2023, for relevant reviews and research articles pertaining to the pathological spread of tau in Alzheimer disease using the search terms: “Alzheimer Disease”, “tau spread”, “tau propagation”, and “tau PET”. Tau pathology has been characterized in Alzheimer disease as a spatiotemporal progression beginning in the entorhinal cortex, then spreading to temporal and prefrontal cortices, and finally large-scale neocortical regions. Studies of tau PET have demonstrated this pattern of spread simultaneous to increased tau burden in early-impacted regions. Ongoing accumulation and spread of tau pathology represent distinct biological processes that are largely entangled with current neuroimaging methods of evaluation with tau PET.

#### Added value of this study

Our research proposes a method of evaluating tau PET that quantifies tau spatial spread separately from pre-specified standard regions evaluating tau burden. We were therefore able to directly compare tau burden and tau spread *in vivo* in relation to the early clinical progression of Alzheimer Disease.

#### Implications of all the available evidence

Our results demonstrate added value of evaluating tau spread in conjunction with tau burden, especially at preclinical and early symptomatic stages of Alzheimer disease. The inclusion of measuring tau spread can benefit clinical trials with tau-targeting drugs in the evaluation of treatment efficacy regarding the success of the drug in slowing or preventing further pathological spread, and therefore slowing or preventing the development of further cognitive deficits.

cortex, then spreading to the temporal cortex and finally isocortical regions following Braak-staging.<sup>19–21</sup> This pattern of spread occurs after amyloid deposition<sup>22</sup> and aligns with widely-accepted cognitive impairments in AD, typically beginning with memory deficits and progressing to executive, visuospatial, and language dysfunction.<sup>14,23</sup> Tau PET studies have provided *in vivo* confirmation of neuropathology findings<sup>24</sup> showing distinct spatiotemporal correlations of tau to regional cortical atrophy<sup>25</sup> and resulting cognitive dysfunction.<sup>26–29</sup> Tau PET uniquely allows for the *in vivo* assessment of spatiotemporal progression, allowing us to evaluate the simultaneous spread of tau pathology to new brain regions and increasing tau levels in previously affected regions. The progression of tau can be characterized by both increasing accumulation of NFTs (tau intensity) and the transportation of tau throughout the brain (tau spatial spread).

Spatial patterns of tau may be explained by prion-like tau seeding of misfolded proteins along synaptically-connected neuronal circuits.<sup>30,31</sup> Transneuronal tau propagation has been supported in cellular research,<sup>32–34</sup> mouse models,<sup>35–38</sup> post-mortem studies,<sup>39</sup> and white matter connectivity.<sup>40,41</sup> This process of spread is activity-dependent, with increased propagation at higher neuronal firing rates,<sup>42–44</sup> resulting in strong correlations of tau within functional networks.<sup>45–47</sup>

Neuroimaging AD research typically measures global tau burden either by defining a threshold for tau<sup>48,49</sup> or by averaging tau PET signal across a pre-defined set of regions of interest (ROIs).<sup>24,50</sup> These summary measures, typically focused on the temporal lobe, capture areas of early sequential tau deposition, but aggregate only a small set of regions rather than specifically considering the degree of spatial spread through the cortex. Some studies have tried to account for spread by evaluating tau PET signal separately within several

ROIs<sup>51,52</sup> while others have been able to model the progression of tau pathology to new regions.<sup>53,54</sup> These analyses do not, however, distinctly differentiate between nor distinctly compare tau intensity and tau spatial spread throughout AD. They additionally force a specific regional structure which is ill suited to subject variability and atypical presentations. Some studies have attempted to address the issue of inter-individual differences and atypical tau spatial patterns but continue to focus on identifying new ROIs and summary measures rather than evaluating tau spread as a separate metric.<sup>55,56</sup>

Disentangling tau intensity and tau spatial spread is important in elucidating which of these biological processes is the driving factor for cognitive decline in AD or whether the amount of tau pathology and spread to other regions interact throughout the disease. With many potential tau-targeting drugs currently being tested in clinical trials,<sup>57</sup> evaluating these components of tau concurrently could be critical for evaluating trial success as well as deciding which drug to deliver. This paper proposes a method for quantifying global tau spatial spread extent, independent from the specific underlying mechanism of protein movement, and characterizes the relationship between tau intensity and tau spatial spread using tau PET in the early stages of AD to determine the efficacy of each biological process as a biomarker for early AD progression.

## Methods

### Participants

Participants enrolled in ongoing studies of memory and aging from the Charles F. and Joanne Knight Alzheimer Disease Research Center (Knight ADRC) at Washington University School of Medicine (WUSM) between 2014 and 2020 were used in our cross-sectional analyses. Inclusion criteria included age 50 and older with amyloid and tau

PET, structural magnetic resonance imaging (MRI), and Clinical Dementia Rating<sup>®58,59</sup> (CDR<sup>®</sup>). All data were collected within a one-year period per participant.

Similar data from a cohort of younger controls (YC, age  $\leq 49$ ) were chosen from both the Knight ADRC and Dominantly Inherited Alzheimer Network (DIAN)-Observational (<https://dian.wustl.edu/our-research/observational-study/>) study at WUSM.<sup>60</sup> All YC from the Knight ADRC were amyloid-negative and cognitively normal as determined by corresponding amyloid PET and CDR. YC from DIAN were amyloid-negative and cognitively normal as well as non-carriers for the *PSEN1*, *PSEN2*, and *APP* genetic mutations studied in DIAN.

Final sample size included all participants from the Knight ADRC and DIAN cohorts who met inclusion criteria, resulting in 445 older participants and 21 younger controls. Participant demographic information was self-reported.

### Ethics

All participants provided written informed consent and the process for data collection was approved by the Washington University Human Research Protection Office, which serves as the central institutional review board (IRB), for the Knight ADRC and DIAN studies (protocols 201106339, 201306009, 201106168, 201106148, and 201409014).

### Imaging acquisition and processing

T1-weighted MRI scans were acquired on a DIAN-approved 3T scanner at a resolution of either  $1 \times 1 \times 1.25 \text{ mm}^3$  or  $1 \times 1 \times 1 \text{ mm}^3$ . Cortical and subcortical ROIs for PET analyses were defined from the structural T1 using FreeSurfer (v5.3-HCP; <http://surfer.nmr.mgh.harvard.edu/>).<sup>61,62</sup>

Amyloid PET imaging was performed using  $10.01 \pm 0.61 \text{ mCi}$  of <sup>18</sup>F-florbetapir (<sup>18</sup>F-AV-45) or  $14.94 \pm 3.85 \text{ mCi}$  of <sup>11</sup>C-Pittsburgh Compound B (<sup>11</sup>C-PiB). Tau PET imaging was performed using  $9.04 \pm 0.86 \text{ mCi}$  of <sup>18</sup>F-flortaucipir (<sup>18</sup>F-AV-1451). For <sup>18</sup>F-AV-45 and <sup>18</sup>F-AV-1451, regional and voxel-specific standard uptake value ratios (SUVRs) were calculated using the cerebellar grey as the reference region for the 50–70 minute and 80–100 minute post-injection window, respectively, using the FreeSurfer-based PET Unified Pipeline (PUP; <https://github.com/ysu001/PUP>).<sup>63</sup> For <sup>11</sup>C-PiB, the post-injection window for SUVR quantification was dependent on the cohort source (30–60 minute for Knight ADRC and 40–70 minute for DIAN).

Global amyloid burden was evaluated with a cortical summary measure by averaging partial volume corrected SUVR across precuneus, prefrontal cortex, gyrus rectus, and lateral temporal cortex ROIs.<sup>62</sup> Amyloid positivity was determined using our previously published thresholds for <sup>18</sup>F-AV-45 (SUVR  $> 1.19$ ) and <sup>11</sup>C-PiB (SUVR  $> 1.42$ ).<sup>62,64</sup>

Centiloid is a commonly used method in the field for standardizing amyloid quantification across tracers and research centers.<sup>65</sup> The cortical summary measures for <sup>18</sup>F-AV-45 and <sup>11</sup>C-PiB were converted to Centiloids per our published equations.<sup>64</sup>

### Clinical testing

Cognitive status was evaluated using the CDR, a clinical tool for assessing the presence and, when present, the severity of Alzheimer dementia. The CDR is calculated based on scores as to whether there has been a change from previously attained levels of function in 6 domains—memory, orientation, judgment and problem solving, community affairs, home and hobbies, and personal care. The global CDR is scored on a scale 0–3 that denotes no impairment (CDR = 0), very mild impairment (CDR = 0.5), mild impairment (CDR = 1), moderate impairment (CDR = 2), and severe impairment (CDR = 3).

### Disease-stage group classification

Participants were assigned to disease-stage groups dependent on amyloid positivity (A $\beta$ +) and cognitive symptoms (CDR), resulting in three final groups for analysis: A $\beta$ -CDR0 (older control, OC), A $\beta$ +CDR0 (pre-clinical AD), and A $\beta$ +CDR>0 (symptomatic AD). Disease-stage groups correspond to early clinical progression of AD, spanning the continuum of amyloid-beta plaque accumulation and cognitive decline.<sup>66</sup>

### Tau Index (TI) and Tau Spatial Spread (TSS)

Tau index (TI) was calculated with PUP-processed tau PET ROI outputs as the mean regional SUVR for the four regions previously identified to characterize early tau accumulation (entorhinal cortex, amygdala, lateral occipital cortex, and inferior temporal cortex).<sup>50</sup> TI was calculated for participants as a measure of tau intensity.

Tau spatial spread (TSS) was measured from voxel-wise tau PET images as the proportion of the relevant brain voxels with abnormal tau pathology (Fig. 1). Image processing and computations specific to the calculation of TSS were conducted with PUP-processed participant files and FMRIB Software Library (FSL v6.0; <https://fsl.fmrib.ox.ac.uk/>).<sup>67</sup>

Participant scans were first preprocessed and co-registered for voxel-wise analyses. T1 MR image, tau PET SUVR image, and FreeSurfer brain mask files were identified for older participants and YCs. MR images underwent automated brain extraction with the Robust Learning-based Brain Extraction System (ROBEX; <https://www.nitrc.org/projects/robex>)<sup>68</sup> for linear and nonlinear transformation<sup>67,69</sup> into common space (MNI152) with 2 mm voxel resampling. MR and SUVR images were registered to MNI152 space with the resulting nonlinear transformation.

Aligned SUVR images for YCs were merged into a four-dimensional matrix and the mean ( $\mu_{\text{vox}}$ ) and

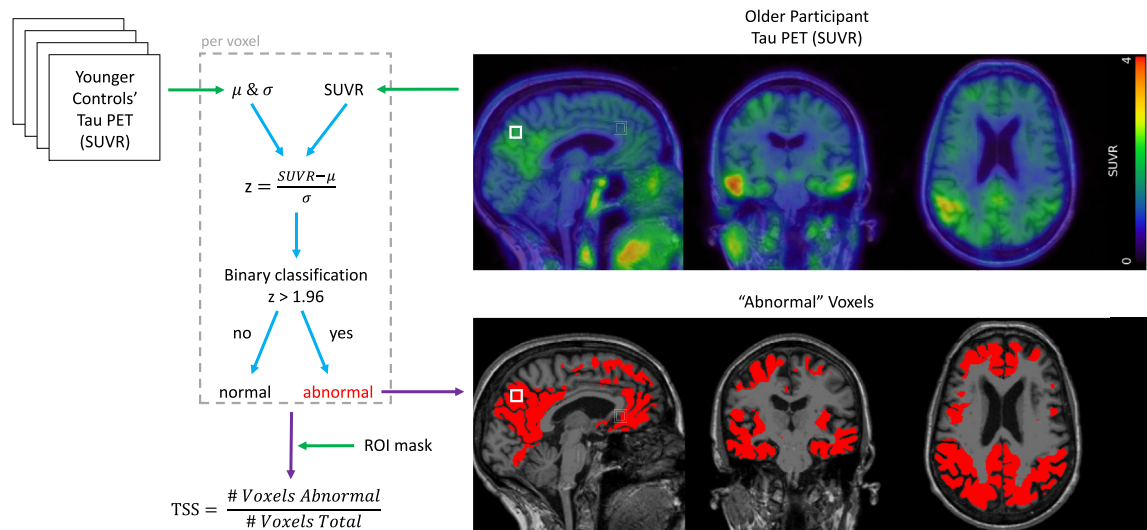


**Fig. 1: Calculation of Tau Spatial Spread.** Tau Spatial Spread (TSS) was calculated for older participants relative to younger controls (YC) using aligned tau PET scans with voxel-wise SUVRs. For each voxel (white square), the SUVR value is identified for the older participant. The SUVR values for the corresponding voxel are identified in all YC scans, which are then used to calculate mean and standard deviation. The older participant's voxel z-score is next calculated from participant SUVR and YC mean and standard deviation. Voxels are then classified as normal or abnormal with the threshold  $z > 1.96$ . Once all voxels have been classified, a region of interest (ROI) mask is applied including the cortex, hippocampus, and amygdala. TSS is calculated as the proportion of abnormal voxels within the ROI mask. All abnormal voxels can be displayed overlaying the participant's MRI.

standard deviation ( $\sigma_{\text{vox}}$ ) were calculated for each voxel. Participant aligned SUVR images were then z-scored for each voxel ( $\text{SUVR}_{\text{vox}}$ ) against corresponding YC voxels ( $z = \frac{\text{SUVR}_{\text{vox}} - \mu}{\sigma}$ ) to produce participant z-score images. These images were then registered back to native space with the original MR image.

Next, individualized brain masks from FreeSurfer were applied to the native z-score images selecting for cortical regions, the hippocampus, and the amygdala. Remaining voxels within this mask were then thresholded for statistical significance ( $z \geq 1.96$ ) relative to YCs and binarized to evaluate whether the voxel has abnormal tau pathology.

TSS was finally calculated as the proportion of abnormal voxels in the brain relative to the total number of candidate voxels ( $\text{TSS} = \frac{\# \text{abnormal voxels}}{\# \text{brain voxels}}$ ).

### Cortical surface projections

Vertex-wise maps were created to visualize tau intensity (Fig. 2a) and tau spread (Fig. 2b) across disease-stage groups using tau PET SUVR images and abnormality masks respectively. Using FSL, participant SUVR image and previously-calculated abnormality mask were co-registered to MNI152 space in the same process as described for TSS and then voxel-wise averages were taken for each disease stage. Tau intensity is depicted as the average tau PET SUVR for each voxel. Tau spread is depicted as the proportion of participants with abnormal tau pathology in each voxel. The data was then projected

onto the cortical surface with an fsaverage template and functions from the nilearn package (v0.10.1) in Python (v3.9.6).

### Statistics

All analyses were conducted with R v4.1.0 with a p-value threshold of  $<0.05$ . Semi-nested linear models referred to as the Four Model Comparison Framework (FMCF) were implemented in these analyses to evaluate the predictive power of TI and TSS separately and conjointly for a variable (X), accounting for covariates age and sex, with the following format: Model 1 ( $X \sim \text{TI} + \text{Covariates}$ ), Model 2 ( $X \sim \text{TSS} + \text{Covariates}$ ), Model 3 ( $X \sim \text{TI} + \text{TSS} + \text{Covariates}$ ), and Model 4 ( $X \sim \text{TI} + \text{TSS} + \text{TI} \times \text{TSS} + \text{Covariates}$ ). Models 1 and 2 are therefore nested in Model 3 which is in turn nested in Model 4, however Models 1 and 2 are not nested within one another. The independent TI (Model 1) and independent TSS (Model 2) models assess the separate predictive ability of TI and TSS. The additive model (Model 3) assesses whether TI and TSS have unique predictive power or whether they provide redundant information with one metric as the better predictor. The interactive model (Model 4) assesses whether TI and TSS interact with one another in addition to independent effects, indicating a more complex and reliant relationship between the biological processes for tau intensity and tau spatial spread. Akaike Information Criterion (AIC) was used for model evaluation.<sup>70</sup>

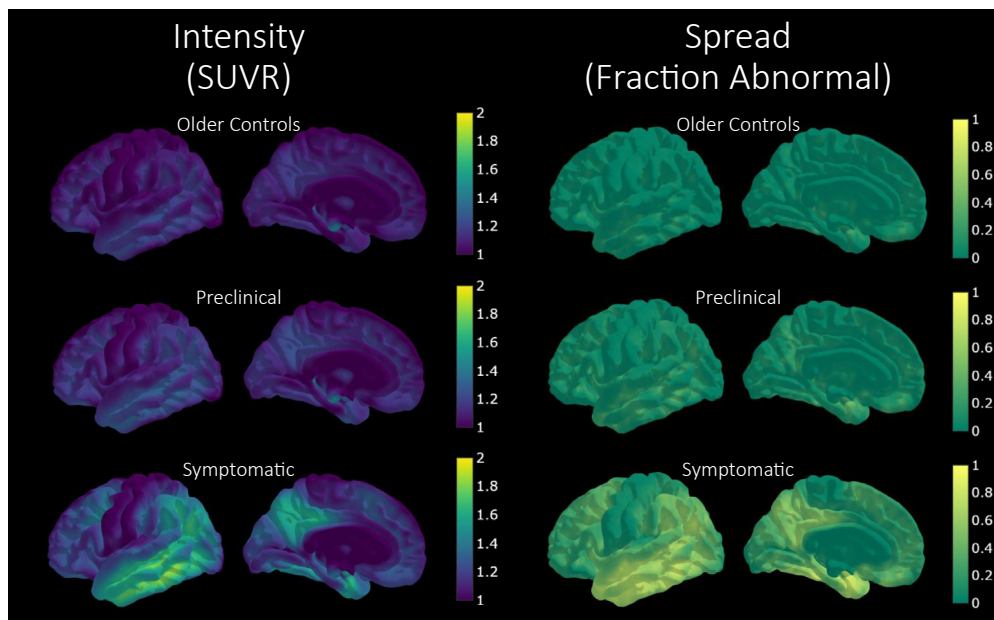


**Fig. 2: Surface projections for tau PET SUVRs and frequency of abnormality across disease stages.** (Left) Voxel-wise tau PET SUVRs averaged across group. Color coded for SUVR (range 1–2). (Right) Voxel-wise group frequency of abnormality, determined by z-scoring against younger controls and thresholding for significance at +1.96. Color coded for the proportion of participants (range 0–1) in which the voxel is “abnormal”.

#### Disease-stage groups

Both tau metrics, TI and TSS, were first evaluated in their ability to discriminate between disease-stage groups. The Kruskal–Wallis test was conducted to determine significant difference in tau metric between disease-stage groups. Post-hoc comparisons were conducted between each group using Dunn’s test with Bonferroni p-value adjustment.

The FMCf was implemented with multinomial logistic regressions predicting disease-stage group to evaluate whether the tau metrics provide unique information for progression through the disease stages. Main effects and interaction were assessed with likelihood-ratio chi-square tests.

If an interaction was found, the relationship between TI and TSS was further dissected by direct comparison. We assessed the correlation between TI and TSS using Spearman correlation generally across all participants and additionally separated by disease-stage group. Changes in correlation across disease stages were assessed using Fisher’s Z Test. Relative amounts of TI and TSS were additionally compared for disease stages by calculating slopes from ranged major axis (RMA) regression<sup>71,72</sup> to account for noise in the measurement of both TI and TSS then compared with 95% confidence interval.

#### Centiloid

TI and TSS were then evaluated relative to amyloid Centiloid as a proxy for time within AD<sup>66,73</sup> in order to

dissect the sensitivity of both tau metrics to within-group changes. We first validated the relationship between Centiloid and both tau metrics across all participants using Pearson correlation. The FMCf was additionally implemented with linear regression predicting Centiloid. Main effects and interaction were assessed with t-tests.

Within-group analyses were then conducted by calculating Pearson correlations between Centiloid and both tau metrics for each disease-stage group to determine which stages show elevated TI and TSS. We then evaluate whether later stages have elevated slope within-stage for TI and TSS, indicating acceleration of tau pathology later in AD, by evaluating the interaction between disease-stage group and Centiloid using F-tests with post-hoc analyses of the interaction using Tukey HSD.

TI and TSS were finally compared for their sensitivity to detecting change in tau pathology within AD after amyloid positivity. TI and TSS were log-transformed for normality then z-scored against the OC group in order to directly compare the tau metrics on the same scale. Local regression via LOESS was used to determine whether z-scored TI (zTI) and TSS (zTSS) visually diverge and at what point along the Centiloid scale. This divergence was then quantified by calculating Z-Score Difference (zTSS—zTI) within individuals and evaluating it against Centiloids with Pearson correlation for all participants and separated by disease-stage group. Sensitivity differences at later time points in AD were

then evaluated by comparing the slopes of the disease-stage groups via interaction between Centiloid and disease-stage group using an F-test and post-hoc analyses of the interaction using Tukey HSD. It is important to note that sensitivity, as evaluated in these analyses, is relative to older controls who are amyloid negative, not based on a histopathology reference standard of tau pathology.

**Role of funders**

The study sponsors had no role in the study design, data collection, data analysis, data interpretation, writing of the report, or the decision to submit the manuscript for publication. All authors had full access to the data in the study and the corresponding author had final responsibility for the decision to submit for publication.

**Results**

Participants from Knight ADRC (n = 445) were included in the study and split into early Alzheimer disease stages. Of these individuals, 255 were classified as OC, 131 as preclinical AD, and 59 as symptomatic AD. 21 YCs were identified between Knight ADRC and DIAN. Participant disease-stage group and YC descriptive statistics are shown in [Table 1](#).

**Disease-stage groups**

TI and TSS were first assessed as separate biomarkers for AD stage ([Fig. 3a and b](#)). Analyses of TI showed a significant main effect for disease stage ( $H(2) = 112.92$ ,

$p < 0.0001$ ). Post-hoc comparisons indicated that mean TI ([Supplementary Table S1](#)) was significantly different between all disease-stage groups. Analyses of TSS likewise showed a significant main effect for disease stage ( $H(2) = 91.96$ ,  $p < 0.0001$ ). Post-hoc comparisons indicated that mean TSS ([Supplementary Table S2](#)) was significantly different between all disease-stage groups. Both TI and TSS therefore demonstrate significantly elevated levels between all disease stages.

The FMCF was used to compare TI and TSS between disease stages ([Table 2](#)). ROC curves for each model are provided in [Supplementary Figure S1](#). The independent models demonstrated that disease stage was predicted significantly by TI alone and by TSS alone. The additive model demonstrated that TI retained significance but TSS was not a significant predictor of diseases stage when modeled with TI. The interactive model showed no significant interaction between TI and TSS. The FMCF indicates higher predictive power of TI than TSS.

TI and TSS were moderately correlated overall ( $R = 0.79$ ,  $p < 0.0001$ ). Correlations were further assessed after splitting participants by disease-stage group ([Fig. 3c](#)). TI and TSS were moderately correlated for OC and preclinical AD groups and highly correlated for the symptomatic AD group. The symptomatic AD group ( $z = -2.75$ ,  $p = 0.0060$ ) and preclinical AD group ( $z = -2.25$ ,  $p = 0.0244$ ) showed significantly higher correlations between TI and TSS compared to the OC group, indicating that TI and TSS become better correlated after amyloid positivity. The relative levels of TI to TSS were further assessed for each disease-stage group ([Supplementary Table S3](#)). The symptomatic AD

	Younger control	Older control	Preclinical AD	Symptomatic AD
N	21	255	131	59
Age (years)	37.54 (10.06)	69.24 (7.98)	71.10 (7.24)	75.01 (6.61)
Sex	-	-	-	-
Male	7 (33%)	128 (50%)	41 (31%)	28 (47%)
Female	14 (67%)	127 (50%)	90 (69%)	31 (53%)
MMSE	29.19 (1.03)	29.29 (1.07)	29.21 (1.20)	25.50 (3.85)
CDR	-	-	-	-
0	21 (100%)	255 (100%)	131 (100%)	-
0.5	-	-	-	45 (76%)
1	-	-	-	13 (22%)
2	-	-	-	1 (2%)
Education (years)	16.28 (2.02)	16.50 (2.33)	16.36 (2.14)	15.52 (2.85)
Race	-	-	-	-
White	14 (67%)	223 (87%)	117 (89%)	55 (93%)
Black	2 (10%)	30 (12%)	12 (9%)	3 (5%)
Other	-	2 (1%)	2 (2%)	1 (2%)
Unknown	5 (24%)	-	-	-

Participant sample size and characteristics for healthy controls and participants, split by disease-stage groups. Data are formatted as n (%) or mean (SD). AD, Alzheimer disease. MMSE, Mini-mental state examination. CDR, Clinical dementia rating.

**Table 1: Participant demographics.**

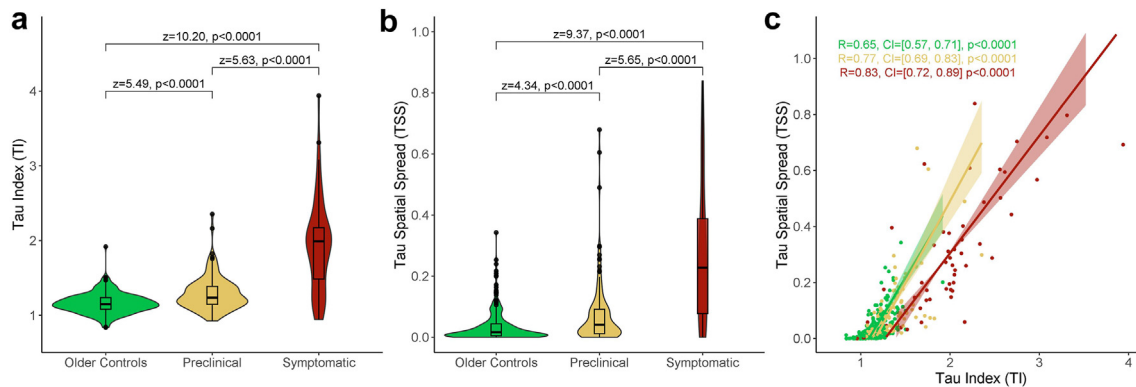


**Fig. 3: Tau Index and Tau Spatial Spread are elevated across disease stages.** (a–b) Comparison of Tau Index (a) and Tau Spatial Spread (b) across disease-stage groups. Pairwise comparisons conducted using Dunn’s test with Bonferroni p-value adjustment (c) Tau Index and Tau Spatial Spread plotted for each disease-stage group with ranged major axis regression and Spearman correlation reported with 95% confidence interval and p-value. Shaded area refers to 95% confidence interval of the regression slope.

group was significantly different from the other two disease-stage groups, demonstrating a higher ratio of TI relative to TSS and indicating a change in relationship between TI and TSS after cognitive impairment is observed.

### Centiloid

Across all participants, TI ( $R = 0.57, p < 0.0001$ ) and TSS ( $R = 0.51, p < 0.0001$ ) were significantly larger at higher Centiloid values. The FMCF was once again used to compare TI and TSS relative to Centiloid (Table 3, Supplementary Tables S4 and S5). The independent models demonstrated significant main effects for both TI and TSS in predicting Centiloid when modeled separately. The additive model demonstrated that when TI and TSS are modeled together, TI retained significance but TSS was not significant. However, the interactive model showed a significant interaction between TI and TSS. TI and TSS are therefore strong predictors of Centiloid independently, but a more complex and interactive relationship is identified between TI and TSS across Centiloids.

Within-group analyses were conducted for TI and TSS across Centiloid. Fig. 4a shows a positive relationship between TI and Centiloid for the preclinical AD and symptomatic AD groups, but not for the OC group. The interaction between Centiloid and disease-stage group was highly significant (Supplementary Table S6), indicating further elevation in TI across Centiloids for later disease stages. Post-hoc pairwise analyses (Supplementary Tables S7 and S8) confirmed significant distinction in slope between OC and preclinical AD, preclinical AD and symptomatic AD, and OC and symptomatic AD groups. Fig. 4b shows a positive relationship between TSS and Centiloid for the preclinical AD and symptomatic AD groups, but not for the OC group. The interaction between Centiloid and disease-stage group was highly significant (Supplementary Table S9). Pairwise analyses (Supplementary Tables S10 and S11) confirmed significant distinction in slope between OC and symptomatic AD as well as between preclinical AD and symptomatic AD groups. However, unlike with TI, significance was not found between OC and preclinical AD groups,

	AIC	Tested variable	df	N	$\chi^2$	p
Groups ~ TI	644.70	TI	2	445	172.78	<0.0001
Groups ~ TSS	649.90	TSS	2	445	122.58	<0.0001
Groups ~ TI + TSS	647.43	TI	2	445	51.47	<0.0001
-	-	TSS	2	445	1.27	0.53
Groups ~ TI + TSS + TI × TSS	649.02	TI	2	445	14.90	0.00026
-	-	TSS	2	445	1.90	0.39
-	-	TI × TSS	2	445	2.41	0.30

Comparison of individual TI, individual TSS, additive, and interactive models predicting disease-stage group. Multinomial logistic regressions with covariates age and sex evaluated with likelihood ratio chi-square tests. Test statistics and significance reported for tested variables as well as evaluation of the model via AIC. TI, Tau Index. TSS, Tau Spatial Spread. AIC, Akaike Information Criterion. df, degrees of freedom.

**Table 2: Disease stage model comparison.**

	AIC	Tested variable	$\beta$	Lower CL	Upper CL	p
Centiloid ~ TI	3437.92	TI	20.50	17.53	23.46	<0.0001
Centiloid ~ TSS	3469.51	TSS	50.93	42.50	59.36	<0.0001
Centiloid ~ TI + TSS	3437.24	TI	16.64	11.15	22.14	<0.0001
-	-	TSS	12.53	-2.53	27.59	0.10
Centiloid ~ TI + TSS + TI $\times$ TSS	3424.32	TI	23.65	17.18	30.12	<0.0001
-	-	TSS	55.65	29.25	82.05	<0.0001
-	-	TI $\times$ TSS	-24.76	-37.31	-12.22	0.00013

Comparison of individual TI, individual TSS, additive, and interactive models predicting Centiloid. Linear regressions evaluated with covariates age and sex with t-tests. Beta coefficient estimates with 95% confidence level and significance reported for tested variables as well as evaluation of the model via AIC. TI, Tau Index. TSS, Tau Spatial Spread. AIC, Akaike Information Criterion. CL, Confidence Limit.

**Table 3: Centiloid model comparison.**

indicating TI is more sensitive than TSS for differences observed between OC and preclinical AD groups.

A deviance was observed between zTI and zTSS relative to Centiloid at the point of amyloid-positivity,<sup>62,64,74</sup> around 20–25 Centiloids (Fig. 4c). The Z-Score Difference was negatively correlated to Centiloids (R = -0.52, p < 0.0001) overall (Fig. 4d). However, this correlation was only maintained within preclinical AD (R = -0.33, p = 0.00011) and symptomatic AD (R = -0.32, p = 0.014) disease stages. The interaction between Centiloid and Group was significant (Supplementary Tables S12–S14). Z-score Difference was therefore elevated within and between disease stages, indicating TI is increasingly more sensitive than TSS throughout AD progression after amyloid positivity.

### Discussion

The progression of tau pathology in AD can be deconstructed into two key components: the spread of tau into new regions (tau spatial spread) and the simultaneous accumulation of NFTs in regions already impacted by tau (tau intensity). The characterization and quantification of these biological processes in tandem using neuroimaging is important for evaluating patient outcomes and predicting subsequent clinical and cognitive decline. The primary goal of these analyses was to propose a method for quantifying tau spatial spread to evaluate and compare tau spatial spread and tau intensity during the early stages of AD.

We found that both tau intensity and tau spread are elevated across all disease stages, beginning as early as the preclinical AD stage. Both tau metrics (TI and TSS) increased relative to amyloid indicating that they are sensitive measures across a continuous scale of disease progression. More tau spread is observed at earlier stages of AD, however tau intensity increases once individuals become symptomatic, at which point TI and TSS are highly correlated. TSS however demonstrates greater variability between subjects, resulting in greater predictive power of TI.

Previous neuroimaging research supports a temporal order of AD biomarkers in which tau pathology begins developing after amyloid positivity but prior to symptom onset,<sup>2,66</sup> thereafter positively correlated with cognitive decline.<sup>15</sup> Our results are consistent with this literature, demonstrating increasingly elevated levels of TI between disease stages, defined by amyloid-beta and cognitive status. We also found positive correlations to amyloid-beta within disease stages after a participant is amyloid-positive indicating that once tau pathology begins, there is an association with amyloid-beta. However, tau progression is not limited to intensity alone. A spatiotemporal order of brain regions impacted by tau pathology has been described following Braak staging simultaneous to the increasing accumulation of NFTs in early-impacted regions.<sup>19,21,75,76</sup> Our results similarly demonstrate elevated TSS in addition to TI across disease stages and amyloid-beta burden. This suggests the general accelerated rate of tau pathology progression after cognitive impairment can be attributed to both increased spread and intensity.

Despite the observation of simultaneous tau spread and tau intensity, the biological mechanisms for these processes suggests a temporal order. Tau is believed to spread primarily via activity-dependent neuronal propagation,<sup>30</sup> however increasing tau intensity with the development of NFTs disrupts neuronal transport and ultimately precipitates cell death.<sup>77</sup> Tau spread therefore necessitates functional active neurons and must precede tau intensity. Consistent with this order, we found relatively higher levels of TSS than TI in the earlier disease stages representative of initial tau pathology development. The finding of early tau spread prior to substantial tau accumulation is supported by previous work in which widespread tau aggregates are found at early Braak stages.<sup>78</sup> Once individuals become symptomatic, however, TI is elevated relative to TSS and the two metrics become strongly correlated. This could be explained by early tau spread impacting substantial regions by this point. The dynamic accumulation of NFTs within such regions ultimately results in an acceleration of tau intensity while tau spread is sustained.



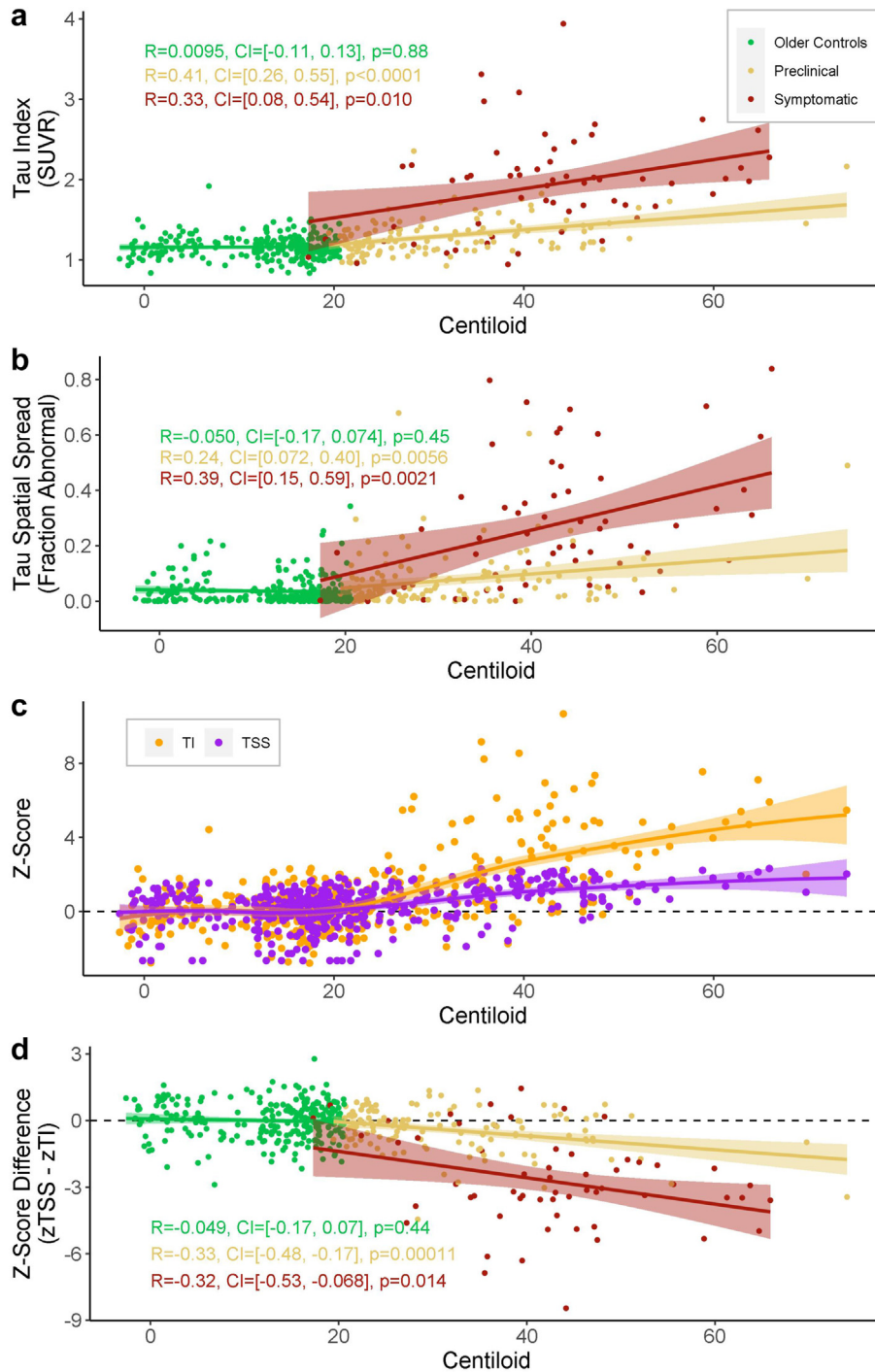


**Fig. 4: Relationship of Tau Index and Tau Spatial Spread relative to amyloid burden.** Tau metrics assessed against Centiloid. Shaded area refers to 95% confidence band. (a–b) TI and TSS for participants relative to Centiloid split by disease-stage group. Pearson correlation reported with 95% confidence interval and p-value. (c) Z-Scored TI and TSS relative to Centiloid with local regression. (d) Divergence of TI and TSS calculated by difference between z-scored TSS and z-scored TI and split by disease-stage group with Pearson correlation.

Evaluating TSS may therefore be important in some cases for identifying early changes in AD prior to cognitive decline. TSS could also be robust to atypical presentations of AD in which tau spread occurs along a different regional pattern than typical amnesic AD.<sup>27,54</sup> While TI is constrained to key regions in typical AD, TSS can capture tau throughout the cortex. This difference between tau metrics is a strength of TSS. However, this lack of constraint also means TSS may capture erroneous tau PET signal or low levels of tau pathology that is not attributed to AD<sup>2,79</sup> as demonstrated in the variability observed in the YC and OC groups (Supplementary Figures S2 and S3). It is important to note however that this variability is likewise observed in the TI metric, with a positive correlation to age potentially indicating Primary Age-Related Tauopathy (PART).<sup>80,81</sup>

The calculation of TSS uses binary classification of whether a voxel is abnormal relative to younger controls. The threshold for each voxel is therefore relatively low and non-AD tau signal may surpass the threshold and classify voxels as abnormal. These false-positive voxels hold equal weight to voxels with much higher AD-related tau signal in the quantification of TSS, introducing potential noise and variability. TI, however, is an intensity-based approach that inherently accounts for the difference in strength of tau signal, minimizing such noise and variability, while additionally selectively including regions characteristic of AD-related tauopathy. TI may therefore be more specific to AD-related tauopathy, which corresponds to our observation of greater variability in TSS than TI within disease stages. This also explains why we find TI is more sensitive than TSS to differences between disease stages.

TI and TSS therefore have complementary strengths and weaknesses and should be used in conjunction for stronger analyses. Individuals with widespread false positives such as those exhibiting diffuse cortical uptake have additionally been identified by comparing relative TI and TSS values (Supplementary Figures S4 and S5).

Due to largely unsuccessful results with amyloid-targeting drugs,<sup>82–84</sup> many clinical trials have changed focus to participants with preclinical AD to prevent or delay symptom onset.<sup>85,86</sup> New tau-targeting drugs have additionally shown promise in animal models<sup>87–90</sup> and are currently in early clinical trial phases.<sup>57</sup> With the surge of these trials, evaluating both TI and TSS may provide additional insight into the success of tau-targeting drugs in reducing or slowing tau progression, particularly in the preclinical stage at which the metrics show the largest divergence.

In interpreting the results of our study, limitations should be considered. The Knight ADRC dataset is skewed towards cognitively normal participants in order to capture early AD-related changes. A longitudinal study with multiple time points of tau PET with participants who progress from preclinical to symptomatic

AD will be an important follow up study. There is also a strong ascertainment bias in which any group of individuals who participate in longitudinal imaging and biomarker studies are not representative of the general population, so these results may not generalize. The limited sample size does not provide the power for analyses evaluating potential confounding factors outside of those included in this paper, which may influence the results and interpretation of this study. Some statistical models are additionally simplified for interpretability, such as the usage of linear regression within the FMCF predicting Centiloid despite violations of the underlying assumptions. Subsequent analyses for the tested relationships support the reported findings despite such violations.

It is important to note that TI and TSS differ in both the method of quantification and the regions assessed. TI is restricted to early regions of interest while TSS accounts for many regions throughout the brain in order to determine whether there is added benefit in evaluating tau spread into additional brain regions. Restricting the regions included in TSS or expanding upon the regions included in TI would allow for more specific analyses between the two metrics, but would likewise reduce the interpretability of the tau metrics regarding their corresponding components of tau pathological progression.

TSS could additionally implement alternative approaches to classify tau positivity at the voxel level such as Gaussian mixture modeling. However, we expect to see a continuum of tau PET SUVRs at the voxel level rather than a clear separation between individuals who are tau-negative and tau-positive since the included cohort encompasses early stages of AD and therefore relatively low levels of tau pathology. Gaussian mixture modeling and similar methods would therefore choose an arbitrary cutoff for tau positivity and be extremely computationally expensive at a voxel-level. We instead chose to classify tau positivity based on a z-score threshold of 1.96 relative to young controls, who are not expected to have tau pathology, because this method identifies when a voxel shows statistically significant SUVRs and therefore abnormally high levels of tau.

Several study strengths result from the chosen method of calculation for TSS. In this study, “abnormal” voxels are identified based on relative SUVR values compared to a younger control group. This method accounts for regional variability in SUVRs not attributed to tau pathology and therefore reduces voxel-wise false positives. When calculating the final value for TSS, an ROI mask is additionally applied to the tau PET scan in order to select for biologically-relevant regions of interest including cortical ROIs, the hippocampus, and the amygdala. The implementation of the ROI mask filters out false positives from off-target PET tracer binding. With the reduction of false positives, TSS better represents AD tau pathology spread extent.

Our results reveal a complex pattern of tau progression in early AD in which tau spatial spread and tau intensity demonstrate different temporal patterns. Tau spatial spread may be captured earlier than tau intensity but shows subject-specific variability that tau intensity is less vulnerable to. Tau intensity increases more rapidly relative to tau spatial spread upon symptom onset and at this point spread and intensity are highly correlated. These results suggest a critical preclinical period in which tau spread and tau intensity behave differently which could have broad applications in preventative tau-targeting clinical trials.

#### Contributors

SD developed the programming scripts, analyzed the data, generated the figures, conducted the literature search, and wrote the manuscript. SD, AM, BAG, and TLSB contributed to method conceptualization. SD, AM, BAG, CDC, NM, DH, and CX developed the statistical approach. SD, AM, BAG, CDC, NM, DH, SK, SF, JS, HS, SJ, KJ, RCH, BMA, CX, AJA, JH, CC, AD, RJB, JCM, and TLSB contributed to data interpretation. TLSB, SK, SF, JS, HS, AD, CC, and RCH oversaw data quality control and processing. TLSB, RJB, AD, CC, and JCM oversaw overall study design and general implementation. AJA, JH, TLSB, RJB, JCM, SJ, AD, CC, and KJ oversaw study implementation and data collection. SD, AM, BAG, CDC, NM, DH, SK, SF, JS, HS, SJ, KJ, RCH, BMA, CX, AJA, JH, CC, AD, RJB, JCM, and TLSB revised the manuscript. This manuscript has been reviewed by DIAN study investigators for scientific content and for consistency of data interpretation with previous DIAN study publications. DIAN investigators oversaw the collection of all demographic, clinical, neuroimaging, and genetic underlying data for participants chosen from the DIAN-Observational study. SD, AM, BAG, and TLSB accessed and verified all included DIAN data. Underlying data from the Knight ADRC was accessed and verified by several authors for included demographic (SD, AM, BAG, TLSB), clinical (SD, AM, BAG, TLSB), and neuroimaging (SD, AM, BAG, TLSB, CDC, SK, SF, JS, HS, RCH) data. Avid Radiopharmaceuticals, Inc., a wholly owned subsidiary of Eli Lilly and Company, enabled use of the 18F-flortaucipir tracer by providing precursor, but did not provide direct funding and was not involved in data analysis or interpretation. All authors contributed substantially to the conception or design of the work or the acquisition of data for the work. All authors reviewed and approved the final manuscript and agree to be accountable for all aspects of the work.

#### Data sharing statement

The data used in these analyses is available upon request for Knight ADRC at <https://knightadrc.wustl.edu/data-request-form/> and for DIAN at <https://dian.wustl.edu/our-research/for-investigators/dian-observational-study-investigator-resources/data-request-form/>.

#### Declaration of interests

Data collection and sharing for this project was supported by the Dominantly Inherited Alzheimer Network (DIAN, U19-AG032438) funded by the National Institute on Aging (NIA), the Alzheimer's Association (SG-20-690363-DIAN), the German Center for Neurodegenerative Diseases (DZNE), the Queen Square Dementia Biomedical Research Centre and the Medical Research Council Dementias Platform UK (MR/L023784/1 and MR/009076/1). Partial support has also been provided by research and development grants for dementia from the Japan Agency for Medical Research and Development (JP22dk0207049), AMED, the Korea Health Technology R&D Project through the Korea Health Industry Development Institute (KHIDI), Korea Dementia Research Center (KDRC) funded by the Ministry of Health & Welfare and Ministry of Science and ICT, Republic of Korea (HI21C0066), the Spanish Institute of Health Carlos III (ISCIII), the Canadian Institutes of Health Research (TAD-125697), the Canadian Consortium of Neurodegeneration and Aging, the Brain Canada Foundation, Fonds de

Recherche du Québec, and the Raul Carrea Institute for Neurological Research (FLENI).

In addition to the acknowledged funding sources for this research, the authors of this manuscript have received financial support from the National Institutes of Health (BMA, TLSB, JH, JCM, CX), National Institute on Aging (AJA, RJB, CC), National Institute of Neurological Disorders and Stroke (RJB), Alzheimer's Association (RJB, CC), DIAN-TU-001 Tau NextGen and OLE (RJB), Biogen (RJB), AbbVie (RJB), Bristol Myers Squibb (RJB), Novartis (RJB), Centene Corporation (RJB), Rainwater Foundation (RJB), Association for Frontotemporal Degeneration FTD Biomarkers Initiative (RJB), BrightFocus Foundation (RJB), Cure Alzheimer's Fund (RJB), Coins for Alzheimer's Research Trust Fund (RJB), Eisai (RJB), The Foundation for Barnes-Jewish Hospital (RJB), TargetALS (RJB), Good Ventures Foundation (RJB), DIAN-TU Pharma Consortium (RJB), Eli Lilly (RJB, TLSB), Avid Radiopharmaceuticals (TLSB), Hoffman-La Roche (RJB), CogState (RJB), Signant (RJB), Siemens (TLSB), and Michael J. Fox Foundation (CC). Travel support was received from Hoffman-La Roche (RJB), Alzheimer's Association Roundtable (RJB), Duke Margolis Alzheimer's Roundtable (RJB), BrightFocus Foundation (RJB), Tau Consortium Investigator's Meeting (RJB), Fondazione Prada (RJB), NAPA Advisory Council on Alzheimer's Research (RJB), and Somalogics (CC). Consultations have been declared for Biogen (TLSB), Eli Lilly (TLSB), Eisai (TLSB), Siemens (TLSB), Bristol Myers Squibb (TLSB), Alector (CC), Circular Genomics (CC), Parabon Nanolabs (JH), Hoffman-La Roche (JH), AlzPath (JH), Prothena (JH), Barcelona Brain Research Center (JCM), Native Alzheimer Disease-Related Resource Center in Minority Aging Research (JCM), and Diadem (CX). Honoraria was received from Korean Dementia Association (RJB), American Neurological Association (RJB), Fondazione Prada (RJB), Weill Cornell Medical College (RJB), Harvard University (RJB), Biogen (TLSB), Eisai (TLSB), Montefiore Grand Rounds NY (JCM), and Tetra-Inst ADRC seminar series Grand Rounds NY (JCM). Patents have been declared for NFL as a marker for ICANs due to CAR-T (BMA), methods for measuring the metabolism of CNS derived biomolecules *in vivo* (RJB), methods for measuring the metabolism of neutrally derived biomolecules *in vivo* (RJB), plasma based methods for detecting CNS amyloid disposition (RJB), plasma based methods for determining A-Beta amyloidosis (RJB), methods of treating based on site-specific tau phosphorylation (RJB), and tau kinetic measurements (RJB). Authors participated on advisory boards for VID (BMA), NNTC (BMA), Hoffman-La Roche/Genentech (RJB), Biogen (RJB), UK Dementia Research Institute at University College London (RJB), Stanford University (RJB), Next Generation Translational Proteomics for Alzheimer's and Related Dementias (RJB), C2N Diagnostics (RJB), Eisai (TLSB), Siemens (TLSB), Eli Lilly (TLSB), Bristol Myers Squibb (TLSB), NIH-sponsored external advisor grants (TLSB), NIA-sponsored Caring Bridge and Wall-E (JH), Cure Alzheimer's Fund Research Strategy Council (JCM), Indiana University LEADS Advisory Board (JCM), and FDA Advisory Committee on Imaging Medical Products (CX). Other declared interests include royalties with equity ownership from C2N Diagnostics (RJB), partnering and receiving stock from Circular Genomics (CC), and being the executive director of DIAN (AD). Participation in the ASNR Alzheimer's and ARIA Study Group, QIBA Amyloid PET Working Group, Alzheimer's Association Clinical Tau PET Work Group, and American College of Radiology/AlzNet Work Group (TLSB). Precursors for radiopharmaceuticals and technology transfer were received from Avid Radiopharmaceuticals/Eli Lilly, LMI, and Cerveau/Lantheus (TLSB). Drugs and services were received from Eisai, Janssen, and Hoffman-La Roche for the DIAN-TU Next Generation Trial and DIAN-TU Gantenerumab Open Label Extension (RJB). All other authors have nothing to disclose.

#### Acknowledgements

Foremost, we wish to acknowledge the dedication of the participants and their families, without whom these studies would not be possible. We additionally thank all of the participating researchers in the Charles F. and Joanne Knight Alzheimer Disease Research Center. We acknowledge the altruism of the participants and their families and

contributions of the DIAN research and support staff at each of the participating sites for their contributions to this study.

#### Appendix A. Supplementary data

Supplementary data related to this article can be found at <https://doi.org/10.1016/j.ebiom.2024.105080>.

#### References

- Jack CR, Bennett DA, Blennow K, et al. NIA-AA Research Framework: toward a biological definition of Alzheimer's disease. *Alzheimers Dement*. 2018;14(4):535–562.
- Jack CR, Bennett DA, Blennow K, et al. A/T/N: an unbiased descriptive classification scheme for Alzheimer disease biomarkers. *Neurology*. 2016;87(5):539–547.
- Morris JC, Storandt M, McKeel DW, et al. Cerebral amyloid deposition and diffuse plaques in “normal” aging: evidence for presymptomatic and very mild Alzheimer's disease. *Neurology*. 1996;46(3):707–719.
- Knopman DS, Petersen RC, Jack CR. A brief history of “Alzheimer disease”: multiple meanings separated by a common name. *Neurology*. 2019;92(22):1053–1059.
- Hardy JA, Higgins GA. Alzheimer's disease: the amyloid cascade hypothesis. *Science*. 1992;256(5054):184–185.
- Nordberg A. PET imaging of amyloid in Alzheimer's disease. *Lancet Neurol*. 2004;3(9):519–527.
- Thal DR, Rüb U, Orantes M, Braak H. Phases of A $\beta$ -deposition in the human brain and its relevance for the development of AD. *Neurology*. 2002;58(12):1791–1800.
- Johnson SC, Christian BT, Okonkwo OC, et al. Amyloid burden and neural function in people at risk for Alzheimer's Disease. *Neurobiol Aging*. 2014;35(3):576–584.
- Braak H, Braak E. Frequency of stages of Alzheimer-related lesions in different age categories. *Neurobiol Aging*. 1997;18(4):351–357.
- Grothe MJ, Barthel H, Sepulcre J, et al. In vivo staging of regional amyloid deposition. *Neurology*. 2017;89(20):2031–2038.
- Brier MR, Gordon B, Friedrichsen K, et al. Tau and A $\beta$  imaging, CSF measures, and cognition in Alzheimer's disease. *Sci Transl Med*. 2016;8(338). [cited 2023 May 16] Available from: <https://www.science.org/doi/10.1126/scitranslmed.aaf2362>.
- Gordon BA, McCullough A, Mishra S, et al. Cross-sectional and longitudinal atrophy is preferentially associated with tau rather than amyloid  $\beta$  positron emission tomography pathology. *Alzheimers Dement*. 2018;10(1):245–252.
- Jagust W. Imaging the evolution and pathophysiology of Alzheimer disease. *Nat Rev Neurosci*. 2018;19(11):687–700.
- Nelson PT, Alafuzoff I, Bigio EH, et al. Correlation of Alzheimer disease neuropathologic changes with cognitive status: a review of the literature. *J Neuropathol Exp Neurol*. 2012;71(5):362–381.
- Sperling RA, Mormino EC, Schultz AP, et al. The impact of A $\beta$  and tau on prospective cognitive decline in older individuals. *Ann Neurol*. 2018;85:181.
- Ossenkoppele R, Hansson O. Towards clinical application of tau PET tracers for diagnosing dementia due to Alzheimer's disease. *Alzheimers Dement*. 2021;17(12):1998–2008.
- Ossenkoppele R, Smith R, Mattsson-Carlgren N, et al. Accuracy of tau positron emission tomography as a prognostic marker in preclinical and prodromal Alzheimer disease: a head-to-head comparison against amyloid positron emission tomography and magnetic resonance imaging. *JAMA Neurol*. 2021;78(8):961.
- Lu M, Pontecorvo MJ, Devous MD, et al. Aggregated tau measured by visual interpretation of flortaucipir positron emission tomography and the associated risk of clinical progression of mild cognitive impairment and Alzheimer disease: results from 2 phase III clinical trials. *JAMA Neurol*. 2021;78(4):445.
- Braak H, Braak E. Neuropathological staging of Alzheimer-related changes. *Acta Neuropathol*. 1991;82(4):239–259.
- Braak H, Braak E. Staging of Alzheimer's disease-related neurofibrillary changes. *Neurobiol Aging*. 1995;16(3):271–278.
- Braak H, Alafuzoff I, Arzberger T, Kretzschmar H, Del Tredici K. Staging of Alzheimer disease-associated neurofibrillary pathology using paraffin sections and immunocytochemistry. *Acta Neuropathol*. 2006;112(4):389–404.
- Price JL, Morris JC. Tangles and plaques in nondemented aging and “preclinical” Alzheimer's disease. *Ann Neurol*. 1999;45(3):358–368.
- Celsis P. Age-related cognitive decline, mild cognitive impairment or preclinical Alzheimer's disease? *Ann Med*. 2000;32(1):6–14.
- Cho H, Choi JY, Hwang MS, et al. In vivo cortical spreading pattern of tau and amyloid in the Alzheimer disease spectrum: tau and Amyloid in AD. *Ann Neurol*. 2016;80(2):247–258.
- La Joie R, Visani AV, Baker SL, et al. Prospective longitudinal atrophy in Alzheimer's disease correlates with the intensity and topography of baseline tau-PET. *Sci Transl Med*. 2020;12(524):eaa5732.
- Day GS, Gordon BA, Jackson K, et al. Tau-PET binding distinguishes patients with early-stage posterior cortical atrophy from amnesic Alzheimer disease dementia. *Alzheimer Dis Assoc Disord*. 2017;31(2):87–93.
- Ossenkoppele R, Schonhaut DR, Schöll M, et al. Tau PET patterns mirror clinical and neuroanatomical variability in Alzheimer's disease. *Brain*. 2016;139(5):1551–1567.
- Schwarz AJ, Yu P, Miller BB, et al. Regional profiles of the candidate tau PET ligand <sup>18</sup>F-AV-1451 recapitulate key features of Braak histopathological stages. *Brain*. 2016;139(5):1539–1550.
- McDonald CR, Gharapetian L, McEvoy LK, et al. Relationship between regional atrophy rates and cognitive decline in mild cognitive impairment. *Neurobiol Aging*. 2012;33(2):242–253.
- Takeda S. Tau propagation as a diagnostic and therapeutic target for dementia: potentials and unanswered questions. *Front Neurosci*. 2019;13:1274.
- Zhang H, Cao Y, Ma L, Wei Y, Li H. Possible mechanisms of tau spread and toxicity in Alzheimer's disease. *Front Cell Dev Biol*. 2021;9:707268.
- Furman JL, Vaquer-Alicea J, White CL, Cairns NJ, Nelson PT, Diamond MI. Widespread tau seeding activity at early Braak stages. *Acta Neuropathol*. 2017;133(1):91–100.
- Abounit S, Wu JW, Duff K, Victoria GS, Zurzolo C. Tunneling nanotubes: a possible highway in the spreading of tau and other prion-like proteins in neurodegenerative diseases. *Prion*. 2016;10(5):344–351.
- Tardivel M, Bégard S, Bousset L, et al. Tunneling nanotube (TNT)-mediated neuron-to neuron transfer of pathological Tau protein assemblies. *Acta Neuropathol Commun*. 2016;4(1):117.
- Clavaguera F, Lavenir I, Falcon B, Frank S, Goedert M, Tolnay M. “Prion-Like” templated misfolding in tauopathies: tau and templated misfolding. *Brain Pathol*. 2013;23(3):342–349.
- de Calignon A, Polydoro M, Suárez-Calvet M, et al. Propagation of tau pathology in a model of early Alzheimer's disease. *Neuron*. 2012;73(4):685–697.
- Liu L, Drouet V, Wu JW, et al. Trans-synaptic spread of tau pathology in vivo. *PLoS One*. 2012;7(2):e31302.
- Gibbons GS, Banks RA, Kim B, et al. GFP-mutant human tau transgenic mice develop tauopathy following CNS injections of Alzheimer's brain-derived pathological tau or synthetic mutant human tau fibrils. *J Neurosci*. 2017;37(47):11485–11494.
- Braak H, Del Tredici K. Spreading of tau pathology in sporadic Alzheimer's disease along cortico-cortical top-down connections. *Cereb Cortex*. 2018;28(9):3372–3384.
- Jacobs HIL, Hedden T, Schultz AP, et al. Structural tract alterations predict downstream tau accumulation in amyloid-positive older individuals. *Nat Neurosci*. 2018;21(3):424–431.
- Watanabe H, Bagarinao E, Yokoi T, et al. Tau accumulation and network breakdown in Alzheimer's disease. In: Takashima A, Wolozin B, Buee L, eds. *Tau biology*. Singapore: Springer Singapore; 2019:231–240 (Advances in Experimental Medicine and Biology; vol. 1184). [cited 2023 Apr 17] Available from: [http://link.springer.com/10.1007/978-981-32-9358-8\\_19](http://link.springer.com/10.1007/978-981-32-9358-8_19).
- Pooler AM, Phillips EC, Lau DHW, Noble W, Hanger DP. Physiological release of endogenous tau is stimulated by neuronal activity. *EMBO Rep*. 2013;14(4):389–394.
- Wu JW, Hussaini SA, Bastille IM, et al. Neuronal activity enhances tau propagation and tau pathology in vivo. *Nat Neurosci*. 2016;19(8):1085–1092.
- Yamada K, Holth JK, Liao F, et al. Neuronal activity regulates extracellular tau in vivo. *J Exp Med*. 2014;211(3):387–393.
- Franzmeier N, Rubinski A, Neitzel J, et al. Functional connectivity associated with tau levels in ageing, Alzheimer's, and small vessel disease. *Brain*. 2019;142(4):1093–1107.
- Franzmeier N, Brendel M, Beyer L, et al. Tau deposition patterns are associated with functional connectivity in primary tauopathies. *Nat Commun*. 2022;13(1):1362.

- 47 Sintini I, Graff-Radford J, Jones DT, et al. Tau and amyloid relationships with resting-state functional connectivity in atypical Alzheimer's disease. *Cereb Cortex*. 2021;31(3):1693–1706.
- 48 Weigand AJ, Eglit GML, Maass A, Bondi MW. What's the cut-point? A systematic review of tau pet thresholding methods: development of new models and analysis methods/tau. *Alzheimers Dement*. 2020;16(S3) [cited 2023 Apr 14] Available from: <https://onlinelibrary.wiley.com/doi/10.1002/alz.046270>.
- 49 Jack CR, Wiste HJ, Schwarz CG, et al. Longitudinal tau PET in ageing and Alzheimer's disease. *Brain*. 2018;141(5):1517–1528.
- 50 Mishra S, Gordon BA, Su Y, et al. AV-1451 PET imaging of tau pathology in preclinical Alzheimer disease: defining a summary measure. *Neuroimage*. 2017;161:171–178.
- 51 Lowe VJ, Wiste HJ, Senjem ML, et al. Widespread brain tau and its association with ageing, Braak stage and Alzheimer's dementia. *Brain*. 2018;141(1):271–287.
- 52 Yaakub SN, Heckemann RA, Keller SS, McGinnity CJ, Weber B, Hammers A. On brain atlas choice and automatic segmentation methods: a comparison of MAPER & FreeSurfer using three atlas databases. *Sci Rep*. 2020;10(1):2837.
- 53 Vogel JW, Iturria-Medina Y, Strandberg OT, et al. Spread of pathological tau proteins through communicating neurons in human Alzheimer's disease. *Nat Commun*. 2020;11(1):2612.
- 54 Vogel JW, , the Alzheimer's Disease Neuroimaging Initiative, Young AL, et al. Four distinct trajectories of tau deposition identified in Alzheimer's disease. *Nat Med*. 2021;27(5):871–881.
- 55 Maass A, Landau S, Baker SL, et al. Comparison of multiple tau-PET measures as biomarkers in aging and Alzheimer's disease. *Neuroimage*. 2017;157:448–463.
- 56 Leuzy A, Binette AP, Vogel JW, et al. Comparison of group-level and individualized brain regions for measuring change in longitudinal tau positron emission tomography in Alzheimer disease. *JAMA Neurol*. 2023;80(6):614.
- 57 Congdon EE, Sigurdsson EM. Tau-targeting therapies for Alzheimer disease. *Nat Rev Neurol*. 2018;14(7):399–415.
- 58 Morris JC. The clinical dementia rating (CDR): current version and scoring rules. *Neurology*. 1993;43(11):2412–2414.
- 59 Hughes CP, Berg L, Danziger W, Coben LA, Martin RL. A new clinical scale for the staging of dementia. *Br J Psychiatry*. 1982;140(6):566–572.
- 60 McKay NS, Gordon BA, Hornbeck RC, et al. Neuroimaging within the Dominantly Inherited Alzheimer's Network (DIAN): PET and MRI. *Neuroscience*; 2022 [cited 2023 May 16]. Available from: <http://biorxiv.org/lookup/doi/10.1101/2022.03.25.485799>.
- 61 Fischl B. FreeSurfer. *Neuroimage*. 2012;62(2):774–781.
- 62 Su Y, D'Angelo GM, Vlassenko AG, et al. Quantitative analysis of PiB-PET with FreeSurfer ROIs. *PLoS One*. 2013;8(11):e73377.
- 63 Su Y, Blazey TM, Snyder AZ, et al. Partial volume correction in quantitative amyloid imaging. *Neuroimage*. 2015;107:55–64.
- 64 Su Y, Flores S, Wang G, et al. Comparison of Pittsburgh compound B and florbetapir in cross-sectional and longitudinal studies. *Alzheimers Dement*. 2019;11(1):180–190.
- 65 Klunk WE, Koeppe RA, Price JC, et al. The Centiloid Project: standardizing quantitative amyloid plaque estimation by PET. *Alzheimers Dement*. 2015;11(1):1.
- 66 Schindler SE, Li Y, Buckles VD, et al. Predicting symptom onset in sporadic Alzheimer disease with amyloid PET. *Neurology*. 2021;97(18):e1823–e1834.
- 67 Woolrich MW, Jbabdi S, Patenaude B, et al. Bayesian analysis of neuroimaging data in FSL. *Neuroimage*. 2009;45(1):S173–S186.
- 68 Iglesias JE, Cheng-Yi L, Thompson PM, Zhuowen T. Robust brain extraction across datasets and comparison with publicly available methods. *IEEE Trans Med Imaging*. 2011;30(9):1617–1634.
- 69 Jenkinson M, Bannister P, Brady M, Smith S. Improved optimization for the robust and accurate linear registration and motion correction of brain images. *Neuroimage*. 2002;17(2):825–841.
- 70 Burnham KP, Anderson DR. Multimodel inference: understanding AIC and BIC in model selection. *Sociol Methods Res*. 2004;33(2):261–304.
- 71 Harper WV. Reduced major Axis regression. In: Kenett RS, Longford NT, Piegorsch WW, Ruggeri F, eds. *Wiley StatsRef: statistics reference online*. 1st ed. Wiley; 2016:1–6 [cited 2023 Nov 28] Available from: <https://onlinelibrary.wiley.com/doi/10.1002/9781118445112.stat07912>.
- 72 Legendre P, Legendre L. *Interpretation of ecological structures. Developments in environmental modelling*. Elsevier; 2012:521–624. [cited 2024 Jan 24] Available from: <https://linkinghub.elsevier.com/retrieve/pii/B9780444538680500101>.
- 73 Betthausen TJ, Kosciak RL, Jonaitis EM, et al. Amyloid time: quantifying the onset of abnormal biomarkers and cognitive impairment along the Alzheimer's disease continuum. *Alzheimers Dement*. 2021;17(S5). [cited 2023 Apr 11] Available from: <https://onlinelibrary.wiley.com/doi/10.1002/alz.056269>.
- 74 Jack CR, Wiste HJ, Weigand SD, et al. Defining imaging biomarker cut points for brain aging and Alzheimer's disease. *Alzheimers Dement*. 2017;13(3):205–216.
- 75 Schultz SA, Gordon BA, Mishra S, et al. Widespread distribution of tauopathy in preclinical Alzheimer's disease. *Neurobiol Aging*. 2018;72:177–185.
- 76 Gordon BA, Friedrichsen K, Brier M, et al. The relationship between cerebrospinal fluid markers of Alzheimer pathology and positron emission tomography tau imaging. *Brain*. 2016;139(8):2249–2260.
- 77 Gendron TF, Petrucelli L. The role of tau in neurodegeneration. *Mol Neurodegener*. 2009;4(1):13.
- 78 Meisl G, Hidari E, Allinson K, et al. In vivo rate-determining steps of tau seed accumulation in Alzheimer's disease. *Sci Adv*. 2021;7(44):eabh1448.
- 79 Jack CR, Knopman DS, Jagust WJ, et al. Tracking pathophysiological processes in Alzheimer's disease: an updated hypothetical model of dynamic biomarkers. *Lancet Neurol*. 2013;12(2):207–216.
- 80 Cray JF, Trojanowski JQ, Schneider JA, et al. Primary age-related tauopathy (PART): a common pathology associated with human aging. *Acta Neuropathol*. 2014;128(6):755–766.
- 81 Hickman RA, Flowers XE, Wisniewski T. Primary age-related tauopathy (PART): addressing the spectrum of neuronal tauopathic changes in the aging brain. *Curr Neurol Neurosci Rep*. 2020;20(9):39.
- 82 Vandenberghe R, Rinne JO, Boada M, et al. Bapineuzumab for mild to moderate Alzheimer's disease in two global, randomized, phase 3 trials. *Alzheimer's Res Ther*. 2016;8(1):18.
- 83 Coric V, Salloway S, van Dyck CH, et al. Targeting prodromal Alzheimer disease with avagacestat: a randomized clinical trial. *JAMA Neurol*. 2015;72(11):1324.
- 84 Doody RS, Raman R, Farlow M, et al. A phase 3 trial of semagacestat for treatment of Alzheimer's disease. *N Engl J Med*. 2013;369(4):341–350.
- 85 Thies W, Bleiler L. 2012 Alzheimer's disease facts and figures Alzheimer's Association \*. *Alzheimers Dement*. 2012;8(2):131–168.
- 86 Mehta D, Jackson R, Paul G, Shi J, Sabbagh M. Why do trials for Alzheimer's disease drugs keep failing? A discontinued drug perspective for 2010-2015. *Expert Opin Investig Drugs*. 2017;26(6):735–739.
- 87 Ke YD, Suchowerska AK, van der Hoven J, et al. Lessons from tau-deficient mice. *Int J Alzheimers Dis*. 2012;2012:1–8.
- 88 Guo T, Noble W, Hanger DP. Roles of tau protein in health and disease. *Acta Neuropathol*. 2017;133(5):665–704.
- 89 Khalil HS, Mitev V, Vlaykova T, Cavicchi L, Zhelev N. Discovery and development of Seliciclib. How systems biology approaches can lead to better drug performance. *J Biotechnol*. 2015;202:40–49.
- 90 del Ser T, Steinwachs KC, Gertz HJ, et al. Treatment of Alzheimer's disease with the GSK-3 inhibitor tideglusib: a pilot study. *J Alzheimers Dis*. 2012;33(1):205–215.